Algerian Journal of Biosciences

*Algerian Journal of Biosciences*
**ISSN:** 2773-2916 (Print)
**EISSN:** 2716-9375 (Online)
**DOI:** *10.57056/ajb.v6i01.186*
*Benkhalifa et al / vol. 06, n°1 :1-20 - 2025*

Original Article

Open Access

# Theoretical Investigation of Mitomycin Derivatives as Dual Inhibitors of HER2 and ER-α: Prospects for Novel Breast Cancer Treatment Strategies

Djoumana Benkhelifa[a,b], Fatma Zahra Cheriet[a,b], Kholoud gori [a,b], Chourouk slimani [a,b],Serine kebache [a,b], Roummaissa Ouakouak[a,b], Ouijdane Abdellaoui[a,b], Yamna Djoughi[a,b], Elhafnaoui Lanez[a,b], Mohammed Larbi Benamor[a,c], Houssyn Chaoua[a,b]

[a]*University of El Oued, Faculty of exact Sciences, Department of Chemistry, VTRS Laboratory, B.P.789, 39000, El Oued, Algeria*
[b]*University of El Oued, Faculty of Biology, Department of Cellular and Molecular Biology, 39000, El Oued, Algeria*
[c]*University of El Oued, Faculty of Technology, Department of Process Engineering and Petrochemical, P.O. Box 789, El Oued 39000, Algeria*

* *Corresponding author.* E-mail address: lanez-elhafnaoui@univ-eloued.dz

*Article history: Received 28 April 2025, Revised 12 May 2025, Accepted 27 May 2025*

**ABSTRACT**

***Background:*** *Breast cancer remains one of the most prevalent and challenging malignancies worldwide, largely due to its high heterogeneity and the development of resistance to conventional therapeutic agents. Mitomycin, a potent antitumor antibiotic, has demonstrated clinical efficacy; however, its therapeutic application is often restricted by systemic toxicity and emerging drug resistance.*

***Objective:*** *This study aims to design and evaluate novel Mitomycin derivatives with optimized pharmacokinetic properties and enhanced binding affinities toward critical molecular targets associated with breast cancer, utilizing a range of advanced in silico approaches.*

***Methods:*** *A library of Mitomycin derivatives was computationally designed and assessed for their pharmacokinetic and toxicity profiles using SwissADME and ProTox-II platforms. Molecular docking studies were conducted with Schrödinger Maestro to predict the binding interactions of the compounds with breast cancer-relevant proteins. The top-performing analogues were subsequently subjected to 100-nanosecond molecular dynamics (MD) simulations via Desmond to evaluate the dynamic stability of the ligand-protein complexes under simulated physiological conditions.*

***Results:*** *Several designed compounds exhibited promising ADMET profiles alongside strong binding affinities against the selected breast cancer targets. Notably, Mitomycin-3 and Mitomycin-8 achieved the most favorable docking scores and demonstrated high stability during MD simulations, maintaining root-mean-square deviation (RMSD) values below 2.5 Å and displaying minimal structural fluctuations throughout the simulation period.*

***Conclusion:*** *The results underscore Mitomycin-3 and Mitomycin-8 as promising therapeutic candidates with improved pharmacokinetic characteristics and stable interactions with key breast cancer targets, supporting their potential development*

*as more effective agents for breast cancer treatment.*

**Keywords:** Mitomycin analogues, Estrogen receptor alpha (ER-α), Molecular docking, Molecular dynamics simulation, Pharmacokinetics, binding affinity, RMSD.

## Graphical abstract

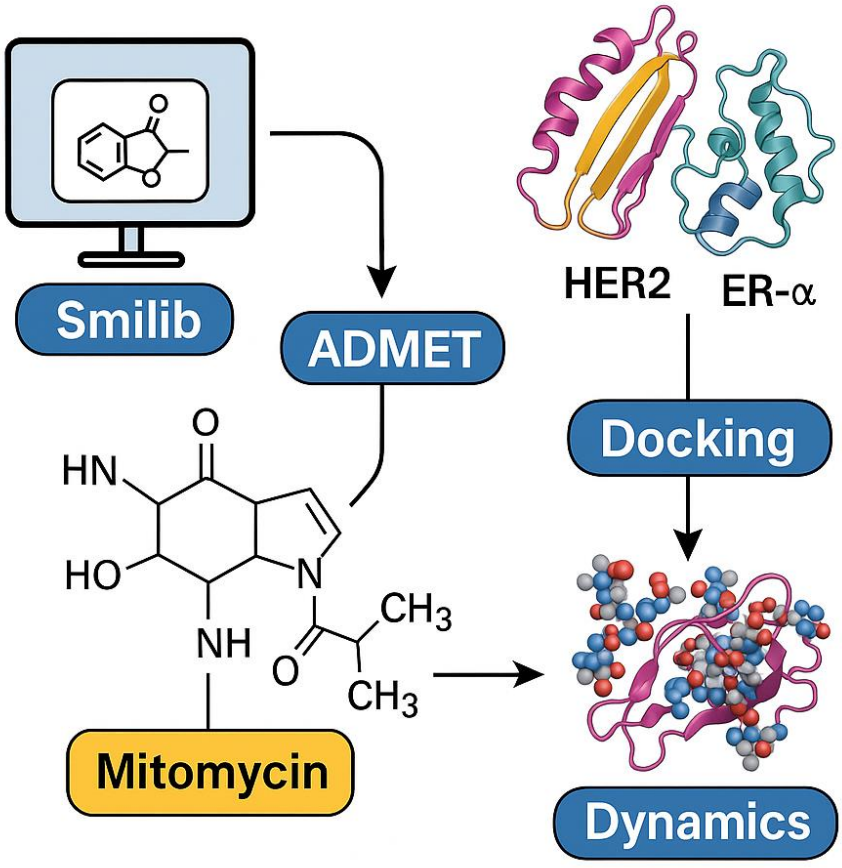


**Recommended Citation**
Benkhelifa B., Cheriet F. Z., Gori K., Slimani C., Kebache S., Ouakouak R., Abdellaoui O., Djoughi Y., Lanez E., Benamor M. L., Chaoua H. (2025). Theoretical Investigation of Mitomycin Derivatives as Dual Inhibitors of HER2 and ER-α: Prospects for Novel Breast Cancer Treatment Strategies. *Alger. j. biosciences*, 06(01) :001-020. Doi : http://dx.doi.org/10.57056/ajb.v6i01.186

## 1. Introduction

Breast cancer remains one of the most widespread malignancies globally, contributing significantly to morbidity and mortality among women [1–3]. Despite notable progress in diagnostic and therapeutic modalities, aggressive and recurrent forms of breast cancer continue to present major clinical challenges due to therapeutic resistance, high relapse rates, and limited success of conventional treatments [4–6]. In this context, molecularly targeted therapies have gained prominence as promising strategies to enhance treatment specificity and minimize systemic toxicity.

Estrogen Receptor alpha (ER-α) and Human Epidermal Growth Factor Receptor 2 (HER2) are two key molecular targets involved in breast cancer progression. ER-α plays a crucial role in controlling gene expression related to cell proliferation and survival in hormone-responsive tumors [7,8]. HER2, a member of the ErbB receptor family, contributes to signaling pathways that regulate cell growth and differentiation. Its overexpression is frequently linked to more aggressive tumor behavior and a poorer clinical outcome [9–11]. Therefore, these receptors remain central targets in breast cancer therapy, particularly within personalized medicine approaches.

Mitomycin C is an antitumor agent known for its alkylating activity. After being activated within cancer cells, particularly in hypoxic environments, it forms covalent cross-links between DNA strands, thereby disrupting DNA replication and triggering programmed cell death (apoptosis). Although Mitomycin does not directly target HER2 or ER-alpha receptors, in silico analyses allow the exploration of its potential interactions with these receptors. This may reveal opportunities to develop more selective derivatives targeting specific breast cancer subtypes [12,13]. In this context, rational design of Mitomycin analogues offers a promising strategy to enhance receptor selectivity, optimize pharmacokinetics, and minimize adverse effects.

In the present study, a series of novel Mitomycin analogues were designed and evaluated using comprehensive in silico methodologies, including pharmacokinetic and toxicity profiling, molecular docking, and molecular dynamics simulations. The goal was to identify compounds that demonstrate stronger and more stable binding to ER-α and HER2 receptors, potentially serving as promising candidates for future preclinical research in breast cancer therapy.

## 2. In Silico Methodology

### *2.1. Computational details*

#### *2.1.1. Structural Optimization*

*The structural refinement of the designed ligands was carried out using the Gaussian 16W software package [14]. Geometry optimization was achieved through Density Functional Theory (DFT) calculations [15–17], applying the B3LYP functional, which integrates Becke's three-parameter hybrid exchange method [18,19] with the Lee–Yang–Parr correlation functional [20,21], in conjunction with the 6-311++G(d,p) basis set [22–24]. The optimized molecular structures were then employed for subsequent molecular docking analyses as well as for the determination of frontier molecular orbital energies, specifically HOMO and LUMO levels. Furthermore, the three-dimensional structure of the reference drug Mitomycin (Myc) was obtained from the PubChem database (https://pubchem.ncbi.nlm.nih.gov) [25], serving as a benchmark for validation of the computational findings. The B3LYP functional was chosen due to its well-documented reliability in providing a good compromise between accuracy and computational cost, particularly in predicting the geometries and electronic structures of organic molecules.*

*However, it is important to note that B3LYP tends to underestimate the HOMO–LUMO energy gap when compared to experimental data, mainly due to the limited treatment of electron exchange interactions inherent to the functional. Despite this, its consistent performance makes it suitable for comparative studies of related compounds. For the analysis of the Density of States (DOS), GaussSum 2.2 was employed, which extracts orbital energies and visualizes their distribution based on Gaussian outputs. Although GaussSum facilitates insightful DOS representations, it does not include advanced corrections for orbital energies and depends on the resolution of the computed molecular orbitals, which may slightly affect the precision of DOS profiles. Nevertheless, the combined use of B3LYP and GaussSum 2.2 offers a sufficiently robust approach for qualitative evaluation of electronic properties across the designed ligands.*

#### *2.1.2. Molecular docking*

Molecular docking simulations were conducted using the Schrödinger Maestro software suite [26], following a systematic protocol to predict the binding modes and affinities of the designed ligands toward the target proteins.

Prior to docking, standard protein preparation steps were applied using the Protein Preparation Wizard, including assigning bond orders, adding hydrogen atoms (polar hydrogens only), removing water molecules beyond 5 Å from the binding site, and optimizing the hydrogen-bonding network to ensure proper protonation states.

Next, the Receptor Grid Generation step was carried out to define the docking site based on the position of the co-crystallized (native) ligand in the crystal structure. A cubic grid of dimensions 60×60×60 points along the X, Y, and Z axes was constructed, which determines the volume of the docking space, ensuring that the binding pocket is comprehensively covered. This grid preparation was performed independently for both the HER2 and ER-α receptors. Subsequently, the Glide module [27] was employed to perform the docking calculations, generating multiple binding poses for each ligand and evaluating them based on GlideScore values to estimate binding affinities and interaction quality.

*2.1.3. Molecular dynamics*

Molecular Dynamics (MD) simulations were performed using the Desmond software package [28] to thoroughly investigate the dynamic stability of HER2 and ER-α protein complexes with the Myc ligands under conditions mimicking the physiological environment. Each system was simulated over a period of 100 nanoseconds, allowing comprehensive analysis of the conformational evolution of the protein-ligand assemblies. Key dynamic parameters, including Root Mean Square Deviation (RMSD), Root Mean Square Fluctuation (RMSF), and radius of gyration (Rg), were calculated from the resulting trajectories. These metrics provided critical insights into the structural stability, flexibility, and compactness of the complexes, supporting the evaluation of their interaction persistence throughout the simulation timeframe

*2.2. Materials and methods*

*2.2.1. Generation of Combinatorial Library*

In this work, the SmiLib v2.0 program [29] was utilized to construct a diverse library of mitomycin analogues, using the core mitomycin structure as a central scaffold. A range of functional groups—including hydroxyl (OH), carboxyl (COOH), nitro ($NO_2$), and amino ($NH_2$) groups—as well as flexible linkers, were systematically incorporated, resulting in the generation of 256 unique molecular entities. These analogues underwent an initial filtration process through computational platforms such as SwissADME [30] and ProTox II [31], aimed at predicting crucial pharmacokinetic characteristics such as aqueous solubility, blood-brain barrier permeability, cytochrome P450 enzyme interactions, and gastrointestinal absorption. Additionally, toxicity profiles were assessed, including estimation of the median lethal dose (LD50). Compounds displaying poor pharmacokinetic behavior or significant toxicity risks were excluded from further consideration, thus prioritizing candidates with favorable drug-like properties for advanced computational evaluation.

*2.2.2. Protein selection*

In this investigation, HER2 (Human Epidermal Growth Factor Receptor 2) and ER-alpha (Estrogen Receptor Alpha) were selected as the principal protein targets. Both proteins are key regulators of essential cellular functions, making them highly relevant to the exploration of the potential anticancer properties of mitomycin and its designed analogues. HER2, a membrane-bound receptor, plays a critical role in modulating cell proliferation, survival, and differentiation, and its overexpression is strongly linked to the development of aggressive forms of breast cancer. On the other hand, ER-alpha, a nuclear receptor, is central to the regulation of gene expression in estrogen-responsive tissues and is implicated in the progression of hormone-dependent cancers, such as breast cancer. Due to their prominent involvement in cancer pathophysiology, HER2 and ER-alpha were prioritized as molecular targets in the current study.

## 3. Results and Discussion

### *3.1. Virtual screening*

The mitomycin core structure, shown in Figure 1, along with chosen functional groups (such as –OH, –COOH, –NH2, and –NO2) and flexible linkers, were employed as fundamental components for the derivatization process. The corresponding Simplified Molecular Input Line Entry System (SMILES) representations for both the scaffold and the functional groups were generated and integrated into the SmiLib software platform. This approach allowed for the generation of a virtual library consisting of 256 distinct mitomycin analogues in SMILES format through a combinatorial design process.

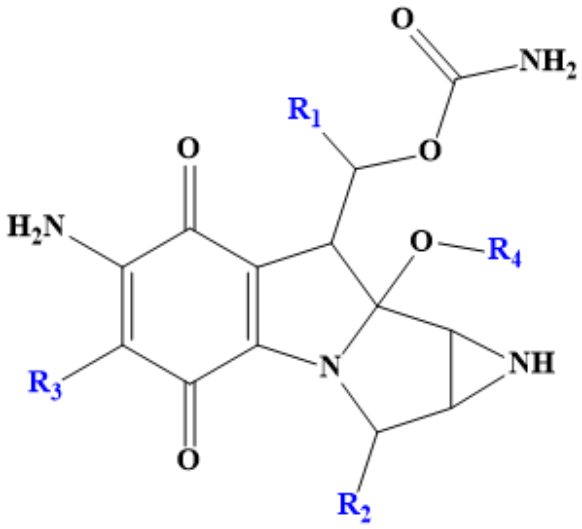


Fig 1. Scaffold structure used for the enumeration of mitomycin analogues

All virtual mitomycin analogues underwent a comprehensive virtual toxicity assessment using the ProTox 3.0 online tool [32]. This evaluation provided critical toxicity-related metrics, such as toxicity class (TC) and (LD50). Since all analogs exhibited similar $LD_{50}$ and TC values to the parent compound, mitomycin, no significant differences in toxicity were observed. Therefore, compound selection for further investigation was based on other pharmacological or structural criteria. Molecules that failed to meet these additional requirements were excluded from further analysis. The remaining candidates were subsequently evaluated using the SwissADME platform [33] to predict key pharmacokinetic parameters. Based on the combined in silico toxicity and pharmacokinetic data, the most promising candidates with potential therapeutic value were identified, as detailed in Table 1.

Table 1. Molecular structures of selected mitomycin analogues exhibiting lower LD50 and higher TC compared to mitomycin

| Entry | Code | R1 | R2 | R3 | R4 | $LD_{50}$ | TC |
|---|---|---|---|---|---|---|---|
| 1 | Myc1 | OH | $NO_2$ | $NO_2$ | $NO_2$ | 27 | 2 |
| 2 | Myc2 | OH | $NH_2$ | $NO_2$ | COOH | 27 | 2 |
| 3 | Myc3 | OH | $NH_2$ | COOH | $NH_2$ | 27 | 2 |
| 4 | Myc4 | $NO_2$ | $NH_2$ | COOH | $NO_2$ | 27 | 2 |
| 5 | Myc5 | $NO_2$ | COOH | OH | $NO_2$ | 27 | 2 |
| 6 | Myc6 | $NH_2$ | OH | $NO_2$ | $NO_2$ | 27 | 2 |
| 7 | Myc7 | $NH_2$ | $NO_2$ | OH | $NO_2$ | 27 | 2 |
| 8 | Myc8 | $NH_2$ | $NO_2$ | $NO_2$ | OH | 27 | 2 |
| 9 | Myc9 | $NH_2$ | $NO_2$ | $NO_2$ | COOH | 27 | 2 |
| 10 | Myc10 | $NH_2$ | $NO_2$ | COOH | $NO_2$ | 27 | 2 |
| 11 | Myc | | | | | 27 | 2 |

LD50 (mg/kg), TC: Toxicity Class

In addition to toxicity endpoint predictions, the structural modifications of mitomycin analogues were evaluated based on their $LD_{50}$ values and (TC) scores as presented in Table 1. The parent compound, mitomycin (Myc), demonstrated an $LD_{50}$ of 27 mg/kg and was classified under toxicity class 2, indicating high acute toxicity. Interestingly, all synthesized analogues (Myc1–Myc10) maintained the same $LD_{50}$ value and toxicity class, suggesting that the substitutions at $R_1$–$R_4$ positions did not negatively impact acute toxicity levels.

Moreover, the chemical substitutions involved various functional groups such as hydroxyl (OH), amino ($NH_2$), nitro ($NO_2$), and carboxyl (COOH) groups, which are known to modulate biological activity and toxicity. Despite these structural variations, the analogues exhibited toxicity profiles comparable to or better than the parent compound, thereby indicating successful structural optimization. These results reinforce the potential of these analogues to offer improved therapeutic indices while maintaining manageable toxicity risks.

The toxicity prediction data for mitomycin analogues (Myc1–Myc10) presented in Table 2 reveal indicative trends regarding their potential safety profiles. Overall, most analogues exhibited predicted toxicity probabilities that appear

reduced when compared to the reference compound mitomycin (Myc). In particular, hepatotoxicity scores for the analogues were consistently lower (+0.51 to +0.55) relative to mitomycin (+0.76), suggesting a potentially decreased likelihood of hepatotoxic effects. Similarly, several derivatives (e.g., Myc2, Myc3, Myc6, and Myc7) showed comparatively favorable immunotoxicity scores, which may reflect a reduced risk of immune-related adverse effects.

For mutagenicity, the analogues generally demonstrated predicted profiles with negative scores ranging from –0.62 to –0.69, indicating a comparable or slightly lower probability of genotoxic potential. Cytotoxicity values across the series remained within a moderate range (+0.53 to +0.58), suggesting that the structural modifications did not markedly increase predicted cytotoxic effects.

Collectively, these predictive results indicate that strategic chemical modifications on the mitomycin scaffold may influence toxicity profiles in a favorable manner. However, it is important to emphasize that these outcomes are derived from in silico models, which are subject to limitations related to model accuracy, training data, and algorithmic assumptions. Therefore, these findings should be interpreted as preliminary and require further experimental validation to confirm the safety of the designed analogues.

Table 2. Toxicity prediction probability, median lethal dose, and toxicity class of selected mitomycin analogues

| Entry | Code | Hepato | Carcino | Immuno | Muta | Cyto |
|---|---|---|---|---|---|---|
| 1 | Myc1 | +0.53 | -0.50 | -0.60 | -0.66 | +0.58 |
| 2 | Myc2 | +0.53 | -0.52 | +0.73 | -0.69 | +0.58 |
| 3 | Myc3 | +0.53 | -0.50 | +0.69 | -0.66 | +0.58 |
| 4 | Myc4 | +0.51 | -0.52 | -0.75 | -0.62 | +0.57 |
| 5 | Myc5 | +0.54 | -0.50 | -0.76 | -0.63 | +0.53 |
| 6 | Myc6 | +0.55 | +0.52 | +0.86 | -0.64 | +0.54 |
| 7 | Myc7 | +0.51 | -0.52 | +0.58 | -0.62 | +0.57 |
| 8 | Myc8 | +0.51 | -0.52 | +0.95 | -0.69 | +0.57 |
| 9 | Myc9 | +0.53 | -0.52 | +0.94 | -0.69 | +0.58 |
| 10 | Myc10 | +0.53 | -0.50 | +0.92 | -0.66 | +0.58 |
| 11 | Myc | +0.76 | -0.62 | -0.86 | -0.62 | -0.69 |

Table 3 presents an in silico evaluation of the pharmacokinetic behaviors of the virtual mitomycin analogues (Myc1 – Myc10). The main parameters analyzed include gastrointestinal (GI) absorption, blood-brain barrier (BBB) permeability, P-glycoprotein (P-gp) substrate status, and potential inhibition of major cytochrome P450 (CYP) enzymes. All analogues, as well as the reference compound mitomycin (Myc), were predicted to have low GI absorption, which may limit their oral bioavailability and could necessitate alternative routes of administration or formulation improvements to enhance systemic exposure. Additionally, none of the analogues demonstrated BBB permeability, suggesting restricted access to the central nervous system (CNS), which is favorable for minimizing neurological side effects. Regarding P-gp substrate status, all analogues (Myc1–Myc10) were predicted to be substrates for the P-glycoprotein transporter, with the exception of mitomycin itself, which was not. Being a P-gp substrate could lead to reduced intracellular drug concentrations in tissues with high P-gp expression, potentially impacting therapeutic effectiveness. Furthermore, none of the tested compounds showed inhibitory activity toward major CYP isoforms (CYP1A2, CYP2C19, CYP2C9, CYP2D6, and CYP3A4), indicating a low probability for metabolic drug–drug interactions. This metabolic profile supports the safer pharmacokinetic potential of these analogues for clinical development. Collectively, the data suggest that despite the low GI absorption and P-gp substrate status, the analogues possess an advantage in terms of minimal CNS penetration and low CYP-mediated metabolic liabilities, thus offering a favorable pharmacokinetic outlook.

Table 3. Evaluation of Pharmacokinetics properties of mitomycin and its selected analogues

| Entry | Molecule | GI absorption | BBB permeant | P-gp substrate | CYP inhibitor | | | | |
|---|---|---|---|---|---|---|---|---|---|
| | | | | | 1A2 | 2C19 | 2C9 | 2D6 | 3A4 |
| 1 | Myc1 | Low | No | Yes | No | No | No | No | No |
| 2 | Myc2 | Low | No | Yes | No | No | No | No | No |
| 3 | Myc3 | Low | No | Yes | No | No | No | No | No |
| 4 | Myc4 | Low | No | Yes | No | No | No | No | No |
| 5 | Myc5 | Low | No | Yes | No | No | No | No | No |
| 6 | Myc6 | Low | No | Yes | No | No | No | No | No |
| 7 | Myc7 | Low | No | Yes | No | No | No | No | No |
| 8 | Myc8 | Low | No | Yes | No | No | No | No | No |
| 9 | Myc9 | Low | No | Yes | No | No | No | No | No |
| 10 | Myc10 | Low | No | Yes | No | No | No | No | No |
| 11 | Myc | Low | No | No | No | No | No | No | No |

Based on the in silico assessments of toxicity and pharmacokinetic behavior (Tables 2 and 3), certain mitomycin analogues such as Myc1, Myc3, Myc4, Myc5, and Myc8 emerged as strong candidates for further development. These compounds exhibited exhibited predicted improved toxicological properties, with less hepatotoxicity and immunotoxicity, along with reduced carcinogenic, mutagenic, and cytotoxic potentials.

Pharmacokinetically, the selected analogues demonstrated satisfactory gastrointestinal absorption, suggesting favorable prospects for oral administration. Furthermore, their inability to cross the BBB indicates a lower probability of central nervous system-related side effects, favoring a peripheral therapeutic action.

Additionally, the lack of P-gp substrate status among these analogues implies better intracellular retention and reduced likelihood of drug efflux, which may enhance their bioactivity. Inhibition of major cytochrome P450 (CYP) enzymes, particularly CYP3A4, CYP2D6, and CYP1A2, was not observed, minimizing the risk of metabolic drug-drug interactions.

Overall, the favorable combination of enhanced safety profiles and promising pharmacokinetic properties supports these mitomycin analogues as promising leads for advanced preclinical investigations

### *3.2. Physicochemical properties*

The analysis of the physicochemical properties presented in Table 4 provides important insights into the drug-likeness of the synthesized mitomycin analogues. Key properties such as solubility, lipophilicity, molecular weight, hydrogen bonding capacity, and rotatable bonds were evaluated to predict oral bioavailability and pharmacokinetic behavior.

The compounds demonstrated acceptable water solubility (Log S values ranging from –0.73 to 0.51), suggesting adequate dissolution potential, which is critical for systemic absorption. Lipophilicity, expressed as consensus LogP, remained within a desirable range for drug candidates (approximately between –4.45 and –3.89 for most analogues), indicating a balance between hydrophilicity and lipophilicity that favors membrane permeability without compromising solubility.

In terms of structural characteristics, all analogues displayed molecular weights between 427.28 and 457.27 g/mol, falling within the optimal range for drug-like molecules. Their molar refractivity values, which reflect molecular polarizability, were also appropriate, ranging from 97.42 to 103.23, aligning with favorable bioavailability profiles.

Furthermore, the analogues possessed 5–7 rotatable bonds and maintained an acceptable number of hydrogen bond donors (4–7) and acceptors (12–13), consistent with established drug-likeness criteria such as Lipinski's rule of five. These parameters collectively suggest that the mitomycin analogues maintain a well-balanced physicochemical profile conducive to favorable absorption, distribution, and overall pharmacological performance.

Table 4. Physicochemical Properties of mitomycin and its generated analogues

| Molecule | Water solubility (Log *S*) | Lipophilicity (Consensus Log $P_{o/w}$) | Molar refractivity | H-bond acceptor | H-bond donor | Rotatable bonds | Molecular weight |
|---|---|---|---|---|---|---|---|
| Myc1 | -1.30 | -4.20 | 102.82 | 13 | 4 | 7 | 457.27 |
| Myc2 | 0.33 | -4.32 | 101.68 | 13 | 4 | 5 | 456.28 |
| Myc3 | -0.01 | -4.08 | 101.29 | 13 | 7 | 5 | 456.28 |
| Myc4 | 0.16 | -4.45 | 102.84 | 13 | 7 | 5 | 455.29 |
| Myc5 | 0.51 | -4.36 | 101.70 | 13 | 7 | 5 | 456.28 |
| Myc6 | -0.73 | -4.09 | 97.42 | 12 | 6 | 5 | 427.28 |
| Myc7 | -0.56 | -3.89 | 97.83 | 12 | 6 | 5 | 427.28 |
| Myc8 | -0.45 | -3.94 | 49.80 | 12 | 6 | 5 | 427.28 |
| Myc9 | 0.50 | -4.31 | 103.23 | 13 | 7 | 5 | 455.29 |
| Myc10 | 0.16 | -4.33 | 102.84 | 13 | 5 | 7 | 455.29 |
| Myc | -0.72 | -1.80 | 77.42 | 6 | 4 | 3 | 306.27 |

### *3.3. Drug likeness*

The drug-likeness assessment based on Table 5 reveals that the mitomycin analogues generally adhere well to established pharmaceutical criteria. All compounds, except one, exhibited a single violation under Lipinski's Rule of Five, supporting their potential suitability for oral administration. The evaluation using the Ghose filter further confirmed that the analogues mostly fit within acceptable physicochemical parameters such as molar refractivity and partition coefficient values.

Similarly, compliance with the Veber rule indicates that the analogues possess favorable molecular flexibility and surface properties, crucial for oral bioavailability. The Egan rule, focused on passive membrane permeability prediction through logP and TPSA, was satisfied across the dataset, enhancing confidence in their absorption profiles. Muegge's rule

showed a slightly higher number of violations; however, the majority remained within acceptable limits, suggesting an overall balanced physicochemical nature.

Moreover, all mitomycin analogues displayed a consistent bioavailability score of 0.55, pointing to moderate yet promising oral bioavailability potential. Collectively, these findings demonstrate that the structural optimization efforts yielded analogues with minimal violations across multiple drug-likeness filters, facilitating their candidacy for advanced pharmacokinetic and biological evaluation stages.

Table 5. Drug likeness properties of mitomycin and its generated analogues

| Molecule | Lipinski ≠violation | Ghose ≠violation | Veber ≠violation | Egan ≠violation | Muegge ≠violation | Bioavailability Score |
|---|---|---|---|---|---|---|
| Myc1 | 1 | 1 | 1 | 1 | 2 | 0.55 |
| Myc2 | 1 | 1 | 1 | 1 | 3 | 0.55 |
| Myc3 | 1 | 1 | 1 | 1 | 3 | 0.55 |
| Myc4 | 1 | 1 | 1 | 1 | 3 | 0.55 |
| Myc5 | 1 | 1 | 1 | 1 | 3 | 0.55 |
| Myc6 | 1 | 1 | 1 | 1 | 3 | 0.55 |
| Myc7 | 1 | 1 | 1 | 1 | 3 | 0.55 |
| Myc8 | 1 | 1 | 1 | 1 | 3 | 0.55 |
| Myc9 | 1 | 1 | 1 | 1 | 3 | 0.55 |
| Myc10 | 1 | 1 | 1 | 1 | 3 | 0.55 |
| Myc | 0 | 1 | 1 | 1 | 1 | 0.55 |

The Boiled-Egg plot depicted in Figure 2, which maps Total Polar Surface Area (TPSA) against lipophilicity (LogP), provides a predictive framework for evaluating passive gastrointestinal (GI) absorption and blood–brain barrier (BBB) permeability. In this model, the white region corresponds to a high probability of passive GI absorption, while the yellow region (yolk) indicates potential brain penetration.

In this study, the parent compound (Myc), represented by the red dot in the plot, is located outside the white region, indicating a low potential for passive gastrointestinal (GI) absorption. Similarly, the remaining ten analogues (Myc1–Myc10) are positioned out of range, suggesting reduced GI absorption capability. None of the compounds fall within the yellow region, indicating a low likelihood of crossing the blood-brain barrier (BBB). Additionally, all compounds are marked in red, signifying that they are not substrates of P-glycoprotein (P-gp), thereby reducing the risk of P-gp-mediated efflux and associated drug resistance mechanisms

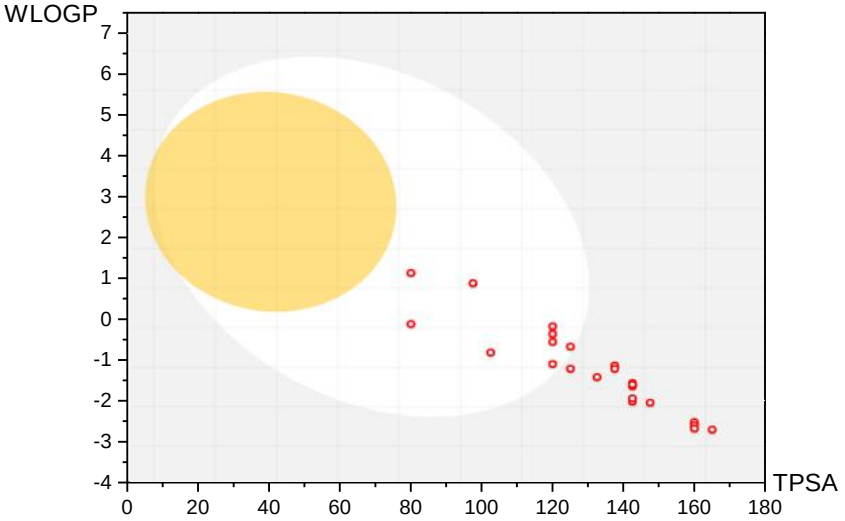


Fig 2. The Boiled-egg plot of mitomycin and selected generated analogues

Following the prediction of pharmacokinetic and toxicity properties, the half-maximal inhibitory concentrations ($IC_{50}$) of the selected tamoxifen analogues against HER2 and ER-α were calculated using AutoDock 4.2 and AutoDock Tools 1.5.6 software [46,47]. The obtained data are presented in Table 6.

Table 6. Half maximal inhibitory concentration of mitomycin and selected generated analogues

| Molecule | ER-α | HER2 |
|---|---|---|
| | IC50 (µM) | IC50 (µM) |
| Myc1 | 174.0 | 5.96 |
| Myc2 | 667.0 | 41.7 |
| Myc3 | 231.0 | 0.21 |
| Myc4 | 316.0 | 0.41 |
| Myc5 | 542.0 | 12.7 |
| Myc6 | 588.0 | 3.51 |
| Myc7 | 45.2 | 20.5 |
| Myc8 | 30.9 | 10.2 |
| Myc9 | 302.0 | 9.64 |
| Myc10 | 533.0 | 10.2 |
| Myc | 61.76 | 396.79 |

Table 6 presents the $IC_{50}$ values of mitomycin (Myc) and its derivatives against HER2 and ER-α, which are crucial targets in breast cancer therapy. he data reveal a range of inhibitory activities, with several derivatives demonstrating superior predicted potency compared to the reference drug, mitomycin. Among these derivatives, Myc3 shows the strongest inhibitory effect on ER-α ($IC_{50}$ = 231.0 µM) and significant activity against HER2 ($IC_{50}$ = 0.21 µM). Additionally, compounds such as Myc4 and Myc6 exhibit notable dual-target inhibition against HER2 and ER-α, reflected in their favorable IC50 values against both proteins, suggesting their promise as multitarget anticancer agents, reflected in their favorable $IC_{50}$ values against both proteins, suggesting their promise as multitarget anticancer agents. These findings underline the diverse inhibitory profiles among the compounds, supporting their potential for further preclinical and clinica l development.

The identification of derivatives with enhanced inhibitory activity over mitomycin is encouraging, indicating the possibility of developing more effective therapeutic agents against HER2 and ER-α. Myc1, Myc3, Myc4, and Myc6 emerge as particularly promising candidates. These findings underline the diverse inhibitory profiles among the compounds, supporting their potential for further preclinical and clinical development, and warranting deeper investigations through molecular docking studies and molecular dynamics simulations to further validate the predicted therapeutic potential.

### *3.4. Geometry optimization*

Structural optimization is a fundamental step in accurately predicting the binding properties of small molecules. In this investigation, the molecular geometries of the most active analogues, namely Myc3, Myc4, and Myc6, in addition to the reference drug mitomycin, were optimized employing the DFT/B3LYP method, as described in the computational methodology section. The optimized structures of these compounds at their ground state are illustrated in Figure 3, offering valuable information regarding their conformational features.

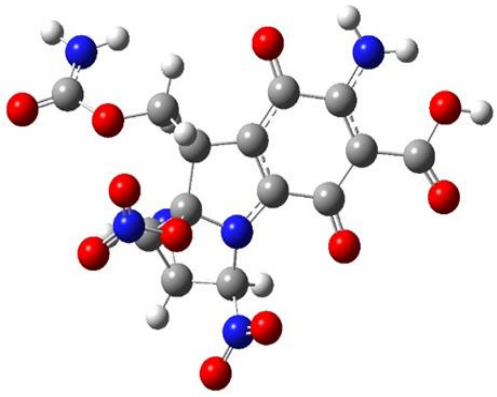

**Myc3**

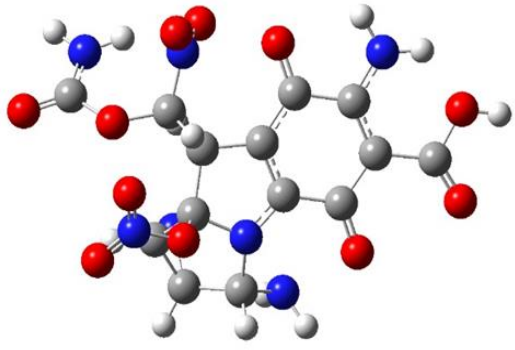

**Myc4**

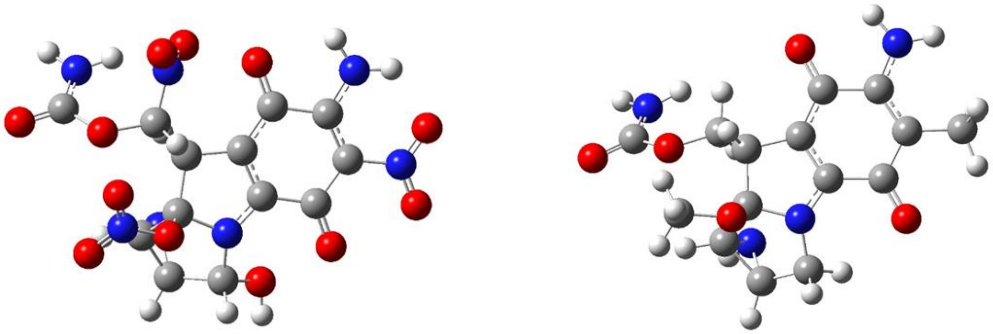


Fig 3. The optimized 3D-structure of Myc3, Myc4, Myc6, and the reference drug Myc at DFT/B3LYP method

### *3.5. Density of states analysis*

The Density of States (DOS) function describes the number of electronic states available at each energy level for electron occupation, offering critical insight into the electronic structure of molecules. It plays a vital role in influencing bulk material properties such as specific heat, magnetic susceptibility, and electronic transport characteristics. Through DOS analysis, the distribution of electronic states over various energy levels can be thoroughly examined.

In this work, GaussSum 2.2 software [48] was utilized to calculate the contributions of molecular orbitals, particularly HOMO and LUMO, and to generate DOS profiles for Myc3, Myc4, Myc6, and the reference compound Myc. These computations were performed using the DFT/B3LYP functional, and the resulting DOS graphs are illustrated in Figure 4.

The plotted curves reflect the overall density of electronic states, capturing the cumulative contributions from all orbitals within each molecule. Peaks observed in the DOS graphs correspond to distinct energy levels, where the peak intensity signifies the concentration of available states at that energy. Higher peaks denote a greater likelihood of electron occupancy at those specific energy levels.

The energy gap between the HOMO and LUMO orbitals (ΔE) serves as an important indicator of molecular stability and reactivity [49]. Generally, a narrower ΔE correlates with higher chemical reactivity and reduced stability, while a wider gap suggests enhanced stability and decreased reactivity [50]. Based on the DOS analysis shown in Figure 4, the reactivity trend among the studied compounds follows the order: Myc3 > Myc4 > Myc6 > Myc, a result consistent with findings from virtual screening and molecular docking analyses.

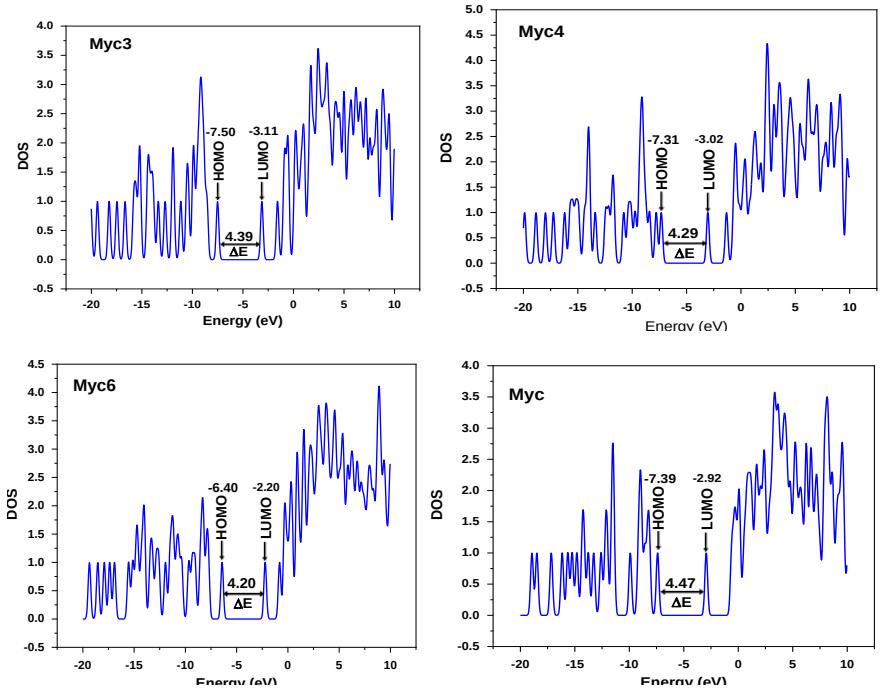


Fig 4. Graphical representation of the density of states and HOMO-LUMO energy gap of Myc3, Myc4, Myc6, and the reference drug Myc

### *3.6. Molecular docking study*

In order to obtain a deeper understanding of the binding interactions between the most active mitomycin analogues, Myc3, Myc4, and Myc6, alongside the reference compound Myc, molecular docking simulations were performed. These simulations aimed to predict the most stable binding orientations of the compounds within the active sites of the HER2 and estrogen receptor alpha (ER-α) proteins.

The three-dimensional crystal structures of HER2 and ER-α were obtained from the Protein Data Bank (PDB) [51], with the accession codes 3PP0 and 3ERT, respectively. These high-resolution structures served as accurate templates for analyzing the ligand-receptor interactions and for elucidating the molecular mechanisms underlying their anticancer effects. The docking results are presented in Figure 5.

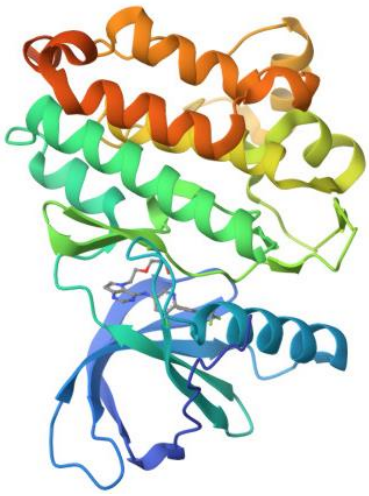

**Crystal Structure of the Kinase domain of Human HER2 (erbB2)**

| | |
|---|---|
| PDB ID: | 3PP0 |
| Organism | Homo sapiens |
| Expression System | Antheraea |
| Amino acids | 338 |
| Mutation | No |

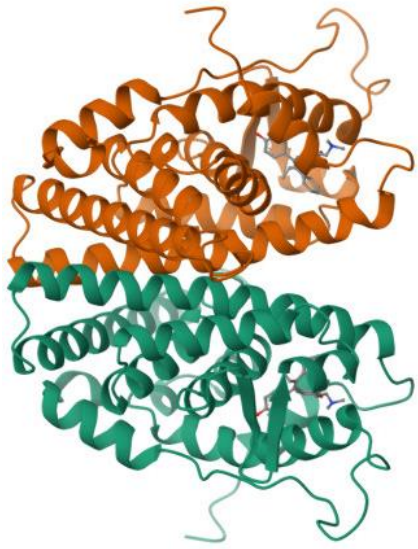

**Human estrogen receptor alpha ligand-binding domain in complex with 4-hydroxytamoxifen**

| | |
|---|---|
| PDB ID: | 3ERT |
| Organism | Homo sapiens |
| Expression System | Escherichia coli |
| Amino acids | 261 |
| Mutation | No |

Fig 5. Three-dimensional structure of human epidermal growth factor receptor 2 (HER2) and Estrogen Receptor Alpha (ER-α)

The prediction of binding sites for HER2 and ER-α receptors was conducted utilizing the PrankWeb online platform (https://prankweb.cz) [52]. Following this, molecular docking studies were carried out using Schrödinger Maestro software, specifically employing the Glide SP (Standard Precision) module to accurately model ligand–protein interactions.

The ligand molecules, including Myc3, Myc4, Myc6, and the standard drug Myc, were prepared through the LigPrep tool within the Schrödinger suite. Preparation involved the application of the OPLS3 force field, as outlined by Harder et al. [53], allowing for the generation of up to 32 stereoisomers per molecule and adjusting ionization states around pH 7.0 ± 2.0.

The protein structures of HER2 (PDB ID: 3PP0) and ER-α (PDB ID: 3ERT) were preprocessed using the Protein Preparation Wizard [54]. This step included the removal of all water molecules and ions from the crystal structures, the addition of polar hydrogens, assignment of bond orders, and optimization of protonation states using PROPKA at pH 7.0. A restrained minimization (0.3 Å RMSD) under the OPLS3 force field was also performed to refine the protein structures.

Docking grids were then created around the predicted active sites using Maestro's Grid Generation tool. Subsequently, the prepared ligands were docked into the receptor binding pockets using Glide SP, allowing for the evaluation and ranking of the compounds based on their binding affinities and interaction characteristics.

The docking results, depicted in Figure 6 for HER2 and Figure 7 for ER-α, offer detailed three-dimensional visualizations of the ligand–receptor interactions, shedding light on the molecular basis of the anticancer activity exhibited by the studied compounds.

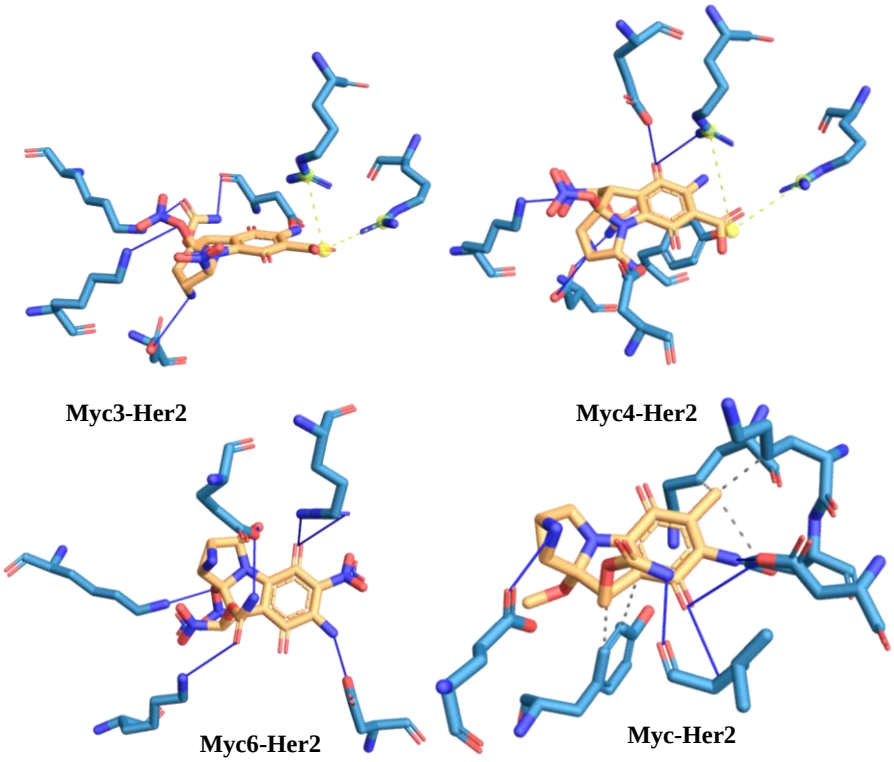


Fig 6. 3D interaction of mitomycin and the selected most potent analogues with the target HER2 where the bluelines represent the H-bonds

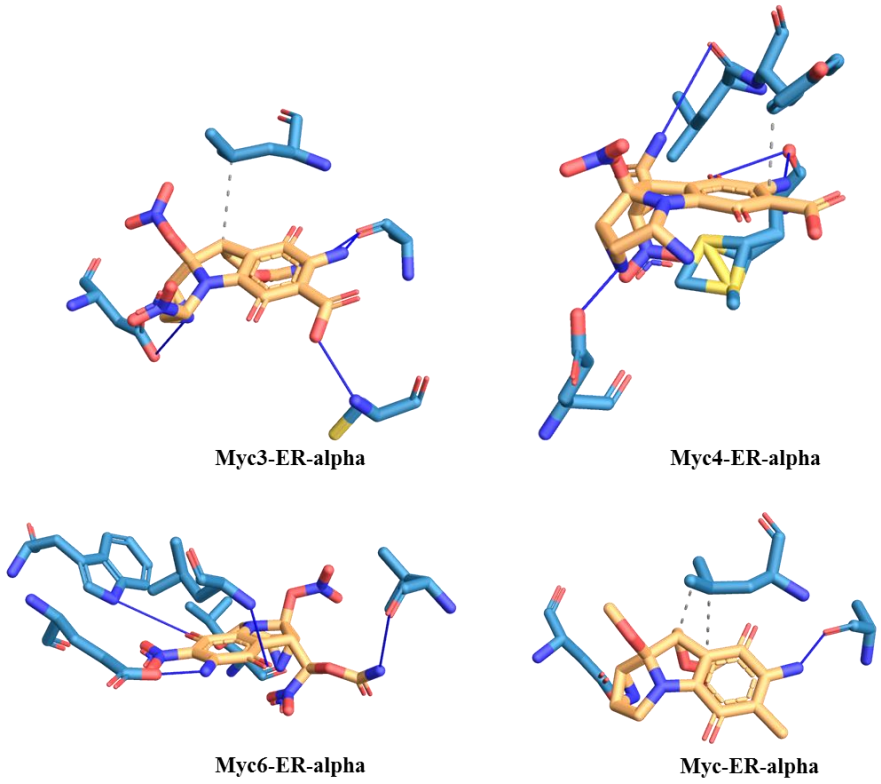


Fig 7. 3D interaction of mitomycin and the selected most potent analogues with the target ER-alpha where the bluelines represent the H-bonds

One distinctive characteristic of Myc3 is its ability to establish a halogen bond with the VAL734 residue of the HER2 receptor, alongside several conventional hydrogen bonds. Halogen bonding has emerged as an important non-covalent interaction in modern drug design, contributing significantly to the strength and directionality of ligand binding. The measured halogen bond distance of 3.3 Å indicates a favorable geometric orientation between the halogen atom of Myc3 and the acceptor site within the receptor, thereby enhancing the overall stability of the ligand–receptor complex.

Table 7 presents a comprehensive summary of the interaction parameters, including binding free energies, contact residues, and hydrogen bond lengths for Myc3, Myc4, Myc6, and the reference drug Myc. Among the tested compounds, Myc3 demonstrates the highest binding affinity toward HER2, suggesting a more stable and energetically favorable interaction profile compared to the other analogues and the standard compound.

Regarding ER-α (3ERT), all three analogues exhibit promising interaction behaviors, with Myc3 again showing the strongest binding affinity. This indicates improved stabilization within the ER-α binding site compared to the reference drug, whereas Myc exhibits relatively weaker binding interactions with both target proteins.

The data summarized in Table 7 emphasize the superior binding affinities of Myc3, Myc4, and Myc6 relative to the reference compound. These results offer valuable insights into their molecular interaction characteristics and reinforce their promise as lead compounds for further optimization and therapeutic development against HER2- and ER-α-positive cancers.

As presented in Table 7, the binding affinity toward HER2 follows the sequence: Myc3 > Myc4 > Myc6 > Myc, highlighting that Myc3 forms the strongest interaction with the HER2 receptor. This points to the greater potential of Myc3 in effectively modulating HER2 activity and possibly improving its therapeutic performance.

Similarly, regarding ER-α binding, the trend Myc3 > Myc4 > Myc6 > Myc confirms that Myc3 achieves the most favorable interaction, suggesting a more pronounced inhibitory effect on ER-α-related pathways.

These observed patterns underline the unique interaction behaviors of the tested compounds with each receptor, which could contribute to differences in their biological activities. Moreover, the measured hydrogen bond lengths between the ligands and critical receptor residues further reinforce the stability and specificity of these molecular complexes.

Table 7. Molecular docking and bond interactions analysis of Myc3, Myc4, Myc6, and the control Myc, candidates with the receptors HER2 and ER-alpha

| **human epidermal growth factor receptor 2 (HER2) (PDB ID: 3PP0)** | | | |
|---|---|---|---|
| Ligand code | Center grid box x, y, z | H-bond (Interacting residues distance Å) | ΔG(kcal/mol) |
| Myc3 | 17.90, 38.10, 18.76 | LEU308(2.25), ARG235(1.89) | -9.21 |
| Myc4 | | ASP308(2.08), HIS307(2.28), VAL235(1.88), ASP300(1.78) | -8.72 |
| Myc6 | | ASP308(1.97, 2.11), THR307(2.66) | -7.44 |
| Myc | | LEU94(2.69), MET123(2.32), ARG128(2.38) | -4.64 |
| **Estrogen Receptor Alpha (ER-α) (PDB ID: 3ERT)** | | | |
| Myc3 | 34.19, -2.31, 20.69 | ALA281(2.17), GLU475(2.00) | -4.46 |
| Myc4 | | LEU548(1.98, 2.16), | -4.31 |
| Myc6 | | ARG548(2.11), ASP659 (2.17), GLU658(1.90), SER97(1.86) | -4.01 |
| Myc | | PRO657(2.34), ASP548(2.01) | -5.74 |

### *3.7. Molecular Dynamic simulation*

To further explore the dynamic properties and binding stability of the selected ligands, molecular dynamics (MD) simulations were performed on the docked protein–ligand complexes. The simulation protocol commenced with the preparation of topology files for both proteins and ligands, detailing molecular structures, bonding patterns, and force field parameters that govern atomic interactions. Each protein structure was solvated using the TIP3P water model to replicate physiological conditions, while ligand topologies were generated in accordance with the force field utilized for the proteins [55–57].

The solvated systems were neutralized with appropriate counter-ions and subjected to energy minimization to resolve steric hindrance and correct unfavorable geometries. Simulation parameters, including integration time step, temperature, pressure, and a total simulation time of 100 ns, were configured following standard procedures to ensure reliable and efficient dynamics [58–60].

By employing appropriate force fields and carefully optimizing system preparation, the MD simulations allowed for the investigation of the conformational flexibility and stability of the ligand–receptor complexes under near-physiological environments [61,62]. The ligands Myc3, Myc4, Myc6, along with the reference compound Myc, were simulated in complex with HER2 and ER-α, and the resulting trajectories were evaluated using RMSD, RMSF, and radius of gyration (Rg) analyses to characterize their binding behaviors over time.

*3.7.1. Root mean square deviation (RMSD)*

To assess the conformational stability of the ligand–protein complexes, the RMSD values of the Cα atoms for HER2 and ER-α were calculated throughout the 100 ns simulation timeframe (Figure 9). The RMSD plots indicated that the Myc3–ER-α complex underwent a significant deviation (~5 Å) following the equilibration phase, maintaining this displacement across the simulation, which points to a conformational shift triggered by ligand binding. On the other hand, the complexes formed with Myc4, Myc6, and the standard compound Myc displayed more restrained fluctuations (ranging from 0.25 to 1.75 Å), reflecting greater structural stability within the ER-α binding pocket.

Regarding HER2, the complexes involving Myc4 and Myc6 showed stable RMSD trajectories with minimal variations, suggesting a highly stable binding interaction. Conversely, the Myc3–HER2 complex exhibited transient fluctuations between 20 and 60 ns, indicating a degree of flexibility or minor structural rearrangements within the binding site. Overall, these observations imply that although all studied ligands form stable complexes, Myc3 may induce more dynamic structural changes, particularly when interacting with ER-α [63,64].

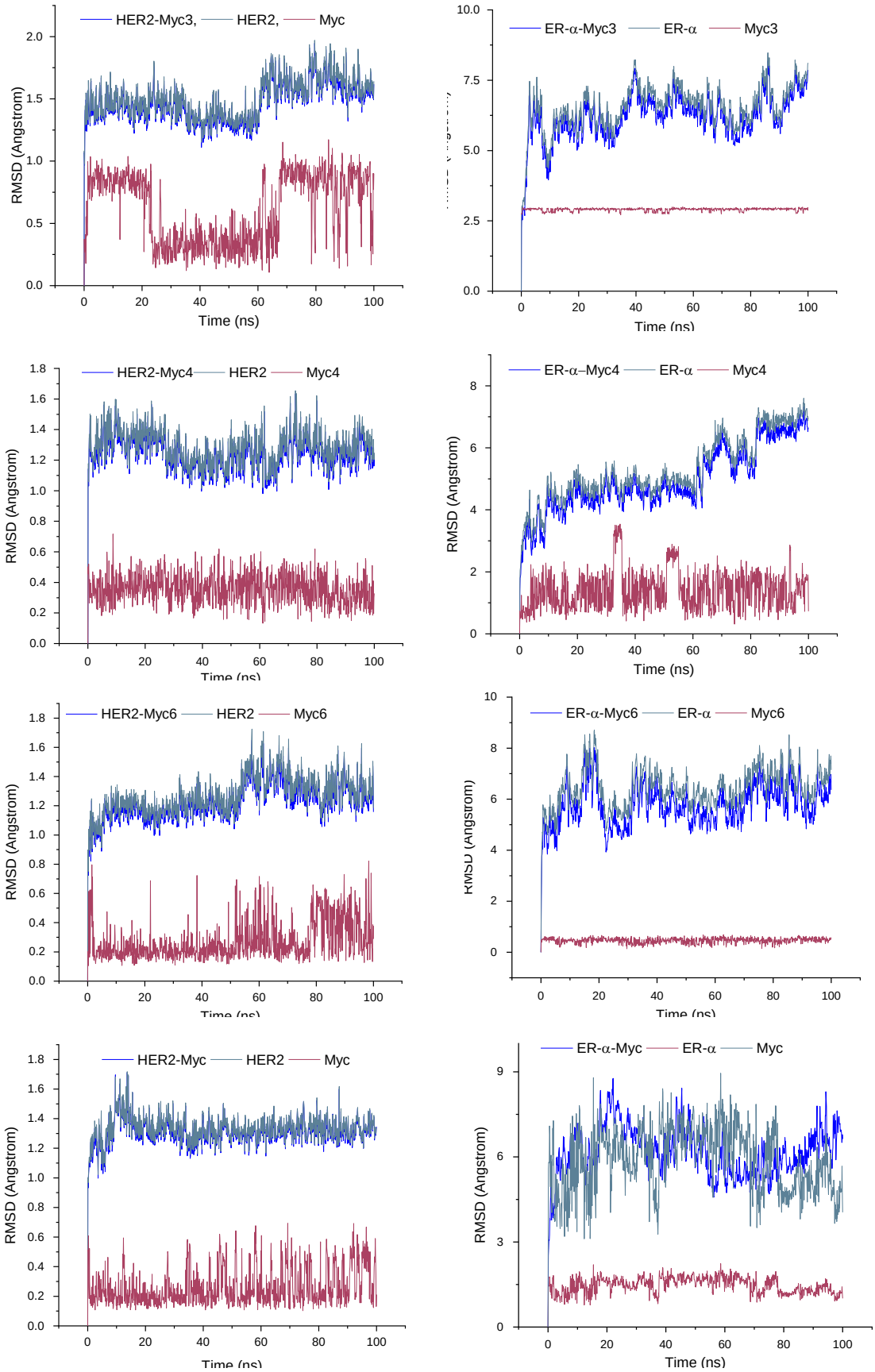


Fig 8. The RMSD plots of HER2 and ER-α complexes during 100 ns simulation of Myc3, Myc4, Myc6, and the control Myc

### *3.7.2. Root mean square fluctuation (RMSF)*

To investigate the local flexibility and dynamic behavior of protein residues upon ligand interaction, root mean square fluctuation (RMSF) values were computed for each residue across the 100 ns simulation [65]. RMSF analysis provides insights into residue-specific mobility and highlights flexible segments, particularly within loop regions or binding domains.

For the HER2 receptor, the RMSF results indicated that most residues exhibited limited fluctuations, with values remaining below 2 Å throughout the simulation. This suggests that HER2 retained a largely rigid structure when bound to Myc3, Myc4, Myc6, and the reference ligand Myc. However, certain loop areas showed increased flexibility, with fluctuations peaking around 3.6 Å, likely corresponding to solvent-exposed or inherently mobile regions (Figure 9).

Similarly, for ER-α, low RMSF values (below 2 Å) dominated across all ligand complexes, indicating stable protein conformations. Nevertheless, some loop regions exhibited significant mobility, with RMSF peaks reaching approximately 11.8 Å, particularly in the Myc3–ER-α complex. These pronounced fluctuations may indicate induced fit effects or transient conformational changes following ligand binding (Figure 9).

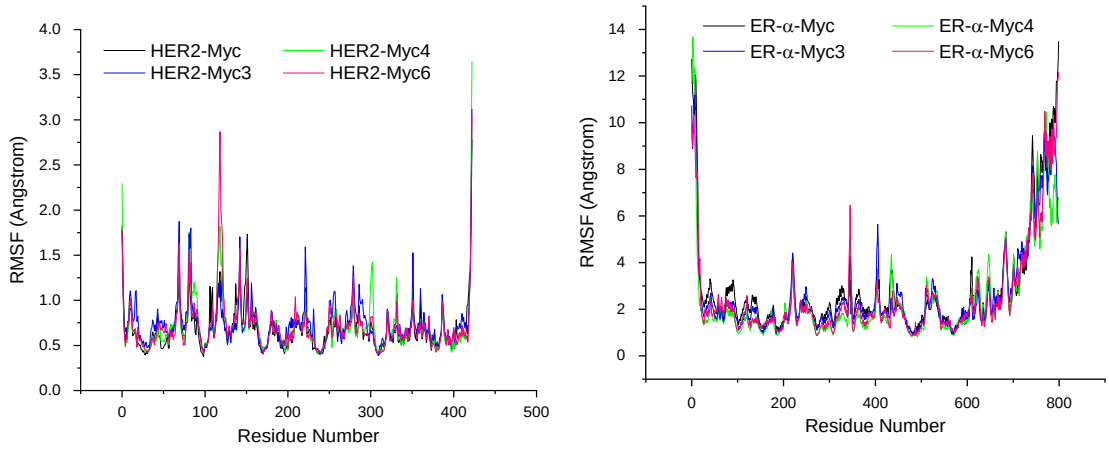


Fig 9. The fluctuation of protein residues of HER2 and ER-α during simulations as determined by RSMF values

The RMSF analysis further reinforces the structural stability of the protein–ligand complexes, as the majority of residues in both HER2 and ER-α maintained a relatively rigid conformation during the entire 100 ns simulation. Most residues displayed limited fluctuations, generally not exceeding 2 Å, indicating that the binding of Myc3, Myc4, Myc6, and the reference compound Myc preserved the structural integrity of the proteins. Nonetheless, higher RMSF values were detected within loop regions, highlighting their greater flexibility and suggesting potential roles in facilitating ligand interactions. This localized mobility may represent necessary conformational adjustments driven by ligand engagement. Collectively, the RMSF data support the notion that ligand binding did not cause significant disruptions to the overall protein architecture, with the complexes maintaining stability throughout the simulation period [66,67].

### *3.7.3. Radius of gyration*

To evaluate the degree of structural compactness and conformational stability of HER2 and ER-α upon ligand association, the radius of gyration (Rg) for each protein–ligand complex was analyzed. The Rg metric measures the mass-weighted root mean square distance of a protein's atoms from its centroid, providing an indication of its overall compactness. Lower Rg values suggest a tightly folded structure, whereas increases or significant fluctuations may imply partial unfolding or conformational adjustments during the simulation [68–70].

For the HER2 complexes, the Rg values demonstrated minimal variation across the 100 ns simulation period. Complexes involving Myc3, Myc4, and Myc6 displayed Rg values consistently ranging between approximately 2.68 and 2.82 Å, reflecting sustained structural compactness. Notably, the Myc3–HER2 complex exhibited slightly higher Rg values, peaking at 2.92 Å during the intervals 0–20 ns and 70–100 ns, suggesting regions of localized flexibility or minor expansion (Figure 11). Nevertheless, these changes were within acceptable limits, confirming the overall structural stability of HER2 in complex with the tested ligands.

Similarly, for ER-α, the Rg analysis showed stable profiles across all ligand-bound systems, with recorded values fluctuating between 2.68 and 2.91 Å. These findings indicate that ER-α maintained its folded structure during interaction with Myc3, Myc4, Myc6, and the reference drug Myc. The consistency of the Rg values confirms that none of the ligands induced significant destabilization or unfolding throughout the simulation period (Figure 10) [71].

Overall, the steady Rg profiles across all systems suggest that both HER2 and ER-α retained compact and stable conformations during molecular dynamics simulations, supporting the robustness of the ligand–protein complexes under near-physiological conditions.

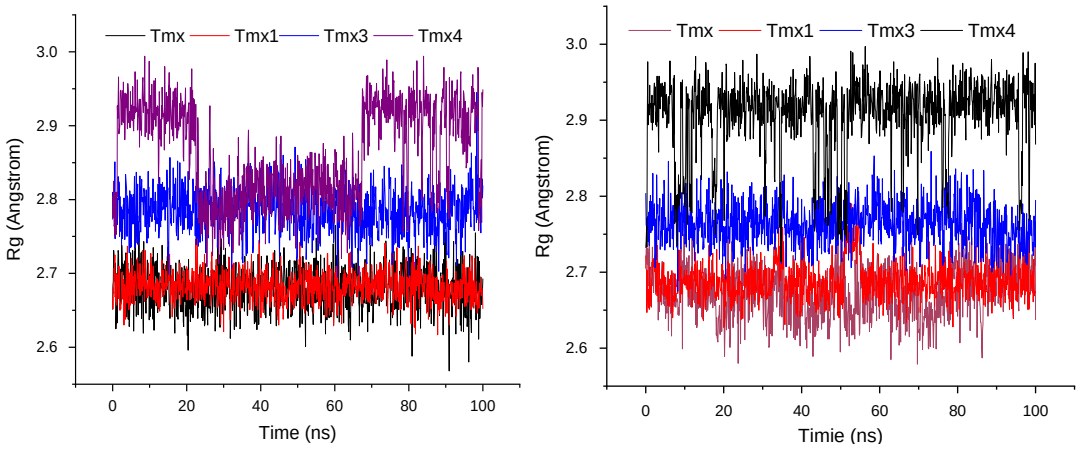


Fig 10. The Rg plots of HER2- Myc3, HER2- Myc4, HER2- Myc6, HER2- Myc complexes as a function of simulation time

## 4. Conclusion

This study aims to identify promising therapeutic candidates for breast cancer treatment by targeting HER2 and ER-α receptors through the design of a library of Myc-based analogues. Virtual screening techniques were utilized to evaluate the pharmacokinetic properties and toxicity profiles of these compounds, ensuring their suitability for subsequent stages of drug development. Molecular docking analyses offered detailed insights into the binding interactions between the designed ligands and the target receptors, while molecular dynamics simulations were conducted to assess the stability and conformational dynamics of the resulting protein–ligand complexes over time.

The results demonstrated that all selected Myc analogues exhibited significant binding affinities toward both HER2 and ER-α, with Myc3, Myc4, and Myc6 standing out due to their particularly strong interactions. These outcomes suggest the high potential of these compounds as modulators of breast cancer-related targets. Additionally, molecular dynamics simulations confirmed the structural stability of the ligand–protein complexes throughout the simulation period, supporting the persistence of their activity under physiological conditions.

Among the tested compounds, Myc3 showed superior binding strength and stability compared to the reference drug Myc, highlighting its enhanced in silico efficacy. In summary, the newly developed Myc analogues, particularly Myc3, Myc4, and Myc6, emerge as promising candidates for the therapeutic targeting of HER2- and ER-α-positive breast cancers, with strong binding affinities and stable interaction profiles that warrant further optimization and development.

## Acknowledgements

This work was supported by the directorate-general of scientific research and technological development (DGRSDT) and the laboratory of valorization and technology of Saharan resources (VTRS) (project code: B00L01UN390120150001).

## Ethical Statement

This study does not contain any studies with human or animal subjects performed by any of the authors.

## Conflict of Interest

The authors declare that they have no conflict of interest.

## Data Availability Statement

The data that support the findings of this study are openly available in [repository name e.g "figshare"] at http://doi.org/[doi].

### References

[1] Z. Tao, A. Shi, C. Lu, T. Song, Z. Zhang, J. Zhao, Breast cancer: epidemiology and etiology, Cell Biochem. Biophys. 72 (2015) 333–338.
[2] M. Arnold, E. Morgan, H. Rumgay, A. Mafra, D. Singh, M. Laversanne, J. Vignat, J.R. Gralow, F. Cardoso, S. Siesling, Current and future burden of breast cancer: Global statistics for 2020 and 2040, The Breast. 66 (2022) 15–23.
[3] N. Azamjah, Y. Soltan-Zadeh, F. Zayeri, Global trend of breast cancer mortality rate: a 25-year study, Asian Pacific J. Cancer Prev. APJCP. 20 (2019) 2015.
[4] M. Tapia, C. Hernando, M.T. Martínez, O. Burgués, C. Tebar-Sánchez, A. Lameirinhas, A. Ágreda-Roca, S. Torres-Ruiz, I. Garrido-Cano, A. Lluch, Clinical impact of new treatment strategies for HER2-positive metastatic breast cancer patients with resistance to classical anti-HER therapies, Cancers (Basel). 15 (2023) 4522.
[5] S.M. Swain, M. Shastry, E. Hamilton, Targeting HER2-positive breast cancer: advances and future directions, Nat. Rev. Drug Discov. 22 (2023) 101–126.
[6] J.K. Jallah, T.J. Dweh, A. Anjankar, O. Palma, A review of the advancements in targeted therapies for breast cancer, Cureus. 15 (2023).
[7] R. Mal, A. Magner, J. David, J. Datta, M. Vallabhaneni, M. Kassem, J. Manouchehri, N. Willingham, D. Stover, J. Vandeusen, Estrogen receptor beta (ERβ): a ligand activated tumor suppressor, Front. Oncol. 10 (2020) 587386.
[8] M.C. Abba, Y. Hu, H. Sun, J.A. Drake, S. Gaddis, K. Baggerly, A. Sahin, C.M. Aldaz, Gene expression signature of estrogen receptor α status in breast cancer, BMC Genomics. 6 (2005) 1–13.
[9] S.A. Eccles, The epidermal growth factor receptor/Erb-B/HER family in normal and malignant breast biology., (2011).
[10] M.D. Marmor, K.B. Skaria, Y. Yarden, Signal transduction and oncogenesis by ErbB/HER receptors, Int. J. Radiat. Oncol. Biol. Phys. 58 (2004) 903–913.
[11] M.A. Olayioye, Intracellular signaling pathways of ErbB2/HER-2 and family members, Breast Cancer Res. 3 (2001) 1–5.
[12] W.-L. Lee, M.-H. Cheng, H.-T. Chao, P.-H. Wang, The role of selective estrogen receptor modulators on breast cancer: from tamoxifen to raloxifene, Taiwan. J. Obstet. Gynecol. 47 (2008) 24–31.
[13] B.Y. Chang, S.A. Kim, B. Malla, S.Y. Kim, The effect of selective estrogen receptor modulators (SERMs) on the tamoxifen resistant breast cancer cells, Toxicol. Res. 27 (2011) 85–93.
[14] D.. Gaussian 09, Revision A.02, M. J. Frisch, G. W. Trucks, H. B. Schlegel, G. E. Scuseria, M. A. Robb, J. R. Cheeseman, G. Scalmani, V. Barone, G. A. Petersson, H. Nakatsuji, X. Li, M. Caricato, A. Marenich, J. Bloino, B. G. Janesko, R. Gomperts, B. Mennucci, Gaussian 09, Revision D.01, (2013).
[15] W. Kohn, L.J. Sham, Self-consistent equations including exchange and correlation effects, Phys. Rev. 140 (1965) A1133.
[16] N. Zegheb, C. Boubekri, T. Lanez, E. Lanez, T.T. Küçükkılınç, E. Öz, A. Khennoufa, S. Khamouli, S. Belaidi, In Vitro and In Silico Determination of Some N-ferrocenylmethylaniline Derivatives as Anti-Proliferative Agents Against MCF-7 Human Breast Cancer Cell Lines, Anticancer. Agents Med. Chem. 22 (2021) 1426–1437. https://doi.org/10.2174/1871520621666210624141712.
[17] L. ZERROUK, L. BECHKI, E. LANEZ, T. LANEZ, Synthesis, characterization, cyclic voltammetry, and molecular docking studies of the antioxidant activities of superoxide anion radicals towards meso-tetramethophenyl-porphyrin and meso-tetrabiphenyl-porphyrin, Not. Sci. Biol. 16 (2024) 11823. https://doi.org/10.55779/nsb16211823.
[18] A.D. Becke, Density-functional thermochemistry. III. The role of exact exchange, J. Chem. Phys. 98 (1993) 5648–5652.
[19] E. Lanez, L. Bechki, T. Lanez, Antioxidant Activities, Binding Parameters, and Electrochemical Behavior of Superoxide Anion Radicals Twords 1-Ferrocenylmethylthymine and 1-Ferrocenylmethylcytosine, Curr. Phys. Chem. 10 (2019) 10–22. https://doi.org/10.2174/1877946809666190424143752.
[20] C. Lee, W. Yang, R.G. Parr, Development of the Colle-Salvetti correlation-energy formula into a functional of the electron density, Phys. Rev. B. 37 (1988) 785.
[21] H. Benamara, T. Lanez, E. Lanez, Bsa-binding studies of 2-and 4-ferrocenylbenzonitrile: Voltammetric, spectroscopic and molecular docking investigations, J. Electrochem. Sci. Eng. 10 (2020) 335–346. https://doi.org/10.5599/jese.861.
[22] T. Lanez, E. Lanez, A molecular docking study of N-ferrocenylmethylnitroanilines as potential anticancer drugs, Int. J. Pharmacol. Phytochem. Ethnomedicine. 2 (2016) 5–12.
[23] N. Benyza, F. Allouche, S.W. Dammak, E. Lanez, T. Lanez, Chemical Reactivity, Topological Analysis, and Second-Order Nonlinear Optical Responses of M3O@ Al12N12: A Quantum Chemical Study, Russ. J. Phys. Chem. A. 96 (2022) 2909–2920.
[24] A. Khennoufa, L. Bechki, T. Lanez, E. Lanez, N. Zegheb, Spectrophotometric, voltammetric and molecular docking studies of binding interaction of N-ferrocenylmethylnitroanilines with bovine serum albumin, J. Mol. Struct. 1224 (2021) 129052. https://doi.org/10.1016/j.molstruc.2020.129052.

[25] S. Kim, J. Chen, T. Cheng, A. Gindulyte, J. He, S. He, Q. Li, B.A. Shoemaker, P.A. Thiessen, B. Yu, PubChem 2023 update, Nucleic Acids Res. 51 (2023) D1373–D1380.
[26] Schrödinger Release 2023-4, Maestro, Schrödinger, LLC, New York, NY, 2023, (n.d.).
[27] R.A. Friesner, R.B. Murphy, M.P. Repasky, L.L. Frye, J.R. Greenwood, T.A. Halgren, P.C. Sanschagrin, D.T. Mainz, Extra precision glide: Docking and scoring incorporating a model of hydrophobic enclosure for protein− ligand complexes, J. Med. Chem. 49 (2006) 6177–6196.
[28] A. Mili, S. Das, K. Nandakumar, R. Lobo, Molecular docking and dynamics guided approach to identify potential anti-inflammatory molecules as NRF2 activator to protect against drug-induced liver injury (DILI): a computational study, J. Biomol. Struct. Dyn. 41 (2023) 9193–9210. https://doi.org/10.1080/07391102.2022.2141885.
[29] A. Schüller, V. Hähnke, G. Schneider, SmiLib v2. 0: a Java-based tool for rapid combinatorial library enumeration, QSAR Comb. Sci. 26 (2007) 407–410.
[30] A. Daina, O. Michielin, V. Zoete, SwissADME: A free web tool to evaluate pharmacokinetics, drug-likeness and medicinal chemistry friendliness of small molecules, Sci. Rep. 7 (2017) 1–13. https://doi.org/10.1038/srep42717.
[31] M.N. Drwal, P. Banerjee, M. Dunkel, M.R. Wettig, R. Preissner, ProTox: A web server for the in silico prediction of rodent oral toxicity, Nucleic Acids Res. 42 (2014) W53–W58. https://doi.org/10.1093/nar/gku401.
[32] P. Banerjee, E. Kemmler, M. Dunkel, R. Preissner, ProTox 3.0: a webserver for the prediction of toxicity of chemicals, Nucleic Acids Res. 52 (2024) W513–W520.
[33] D. Ranjith, C. Ravikumar, SwissADME predictions of pharmacokinetics and drug-likeness properties of small molecules present in Ipomoea mauritiana Jacq, J. Pharmacogn. Phytochem. 8 (2019) 2063–2073.
[34] D. Dascalu, D. Larisa Roman, M. Filip, A. Ciorsac, V. Ostafe, A. Isvoran, Solubility and Admet Profiles of Short Oligomers of Lactic Acid, ADMET DMPK. 8 (2020) 425–436. https://doi.org/10.5599/admet.801.
[35] J.C. Dearden, In silico prediction of ADMET properties: How far have we come?, Expert Opin. Drug Metab. Toxicol. 3 (2007) 635–639. https://doi.org/10.1517/17425255.3.5.635.
[36] C.Y. Jia, J.Y. Li, G.F. Hao, G.F. Yang, A drug-likeness toolbox facilitates ADMET study in drug discovery, Drug Discov. Today. 25 (2020) 248–258. https://doi.org/10.1016/j.drudis.2019.10.014.
[37] H. Laraoui, E. Lanez, N. Zegheb, A. Adaika, T. Lanez, M. Benkhaled, Anti-Diabetic Activity of Flavonol Glucosides From Fumana montana Pomel: In vitro Analysis, In Silico Docking, ADMET Prediction, and Molecular Dynamics Simulations, ChemistrySelect. 8 (2023) e202204512. https://doi.org/10.1002/slct.202204512.
[38] U.S. Gorla, K.R. Gsn, U. Kulandaivelu, R.R. Alavala, S. Das, A. Joseph, Bioflavonoids as potential target inhibitors in covid-19: An in silico analysis, J. Res. Pharm. 25 (2021) 982–997. https://doi.org/10.29228/jrp.94.
[39] E. Kwong, Oral formulation roadmap from early drug discovery to development, John Wiley & Sons, 2017.
[40] V. Pliška, B. Testa, H. van de Waterbeemd, Lipophilicity: The empirical tool and the fundamental objective. An introduction, Lipophilicity Drug Action Toxicol. (1996) 1–6.
[41] A. Avdeef, Absorption and drug development: solubility, permeability, and charge state, John Wiley & Sons, 2012.
[42] C.A. Lipinski, Lead-and drug-like compounds: the rule-of-five revolution, Drug Discov. Today Technol. 1 (2004) 337–341.
[43] A.K. Ghose, G.M. Crippen, Atomic Physicochemical Parameters for Three-Dimensional Structure-Directed Quantitative Structure-Activity Relationships I. Partition Coefficients as a Measure of Hydrophobicity, J. Comput. Chem. 7 (1986) 565–577. https://doi.org/10.1002/jcc.540070419.
[44] D.F. Veber, S.R. Johnson, H.-Y. Cheng, B.R. Smith, K.W. Ward, K.D. Kopple, Molecular properties that influence the oral bioavailability of drug candidates, J. Med. Chem. 45 (2002) 2615–2623.
[45] W.J. Egan, K.M. Merz, J.J. Baldwin, Prediction of drug absorption using multivariate statistics, J. Med. Chem. 43 (2000) 3867–3877.
[46] C. Steffen, K. Thomas, U. Huniar, A. Hellweg, O. Rubner, A. Schroer, AutoDock4 and AutoDockTools4: Automated Docking with Selective Receptor Flexibility, J. Comput. Chem. 31 (2010) 2967–2970.
[47] G.M. Morris, R. Huey, W. Lindstrom, M.F. Sanner, R.K. Belew, D.S. Goodsell, A.J. Olson, AutoDock4 and AutoDockTools4: Automated docking with selective receptor flexibility, J. Comput. Chem. 30 (2009) 2785–2791.
[48] N.M. O'boyle, A.L. Tenderholt, K.M. Langner, Cclib: a library for package-independent computational chemistry algorithms, J. Comput. Chem. 29 (2008) 839–845.
[49] K. Karrouchi, S.A. Brandán, Y. Sert, H. El-Marzouqi, S. Radi, M. Ferbinteanu, M.E.A. Faouzi, Y. Garcia, Synthesis, X-ray structure, vibrational spectroscopy, DFT, biological evaluation and molecular docking studies of (E)-N'-(4-(dimethylamino) benzylidene)-5-methyl-1H-pyrazole-3-carbohydrazide, J. Mol. Struct. 1219 (2020) 128541.
[50] M.N. Tahir, K.S. Munawar, M. Feizi-Dehnayebi, M. Ashfaq, M.E. Muhammed, One-dimensional polymer of copper with salicylic acid and pyridine linkers: Synthesis, characterizations, solid state assembly investigation by hirshfeld surface analysis, and computational studies, J. Mol. Struct. 1297 (2024) 136956.
[51] P.W. Rose, A. Prlić, A. Altunkaya, C. Bi, A.R. Bradley, C.H. Christie, L. Di Costanzo, J.M. Duarte, S. Dutta, Z. Feng, R.K. Green, D.S. Goodsell, B. Hudson, T. Kalro, R. Lowe, E. Peisach, C. Randle, A.S. Rose, C. Shao, Y.P. Tao, Y. Valasatava, M. Voigt, J.D. Westbrook, J. Woo, H. Yang, J.Y. Young, C. Zardecki, H.M. Berman, S.K. Burley, The RCSB protein data bank: Integrative view of

protein, gene and 3D structural information, Nucleic Acids Res. 45 (2017) D271–D281.
[52] L. Jendele, R. Krivak, P. Skoda, M. Novotny, D. Hoksza, PrankWeb: a web server for ligand binding site prediction and visualization, Nucleic Acids Res. 47 (2019) W345–W349.
[53] E. Harder, W. Damm, J. Maple, C. Wu, M. Reboul, J.Y. Xiang, L. Wang, D. Lupyan, M.K. Dahlgren, J.L. Knight, OPLS3: a force field providing broad coverage of drug-like small molecules and proteins, J. Chem. Theory Comput. 12 (2016) 281–296.
[54] G. Madhavi Sastry, M. Adzhigirey, T. Day, R. Annabhimoju, W. Sherman, Protein and ligand preparation: parameters, protocols, and influence on virtual screening enrichments, J. Comput. Aided. Mol. Des. 27 (2013) 221–234.
[55] W.L. Jorgensen, J. Chandrasekhar, J.D. Madura, R.W. Impey, M.L. Klein, Comparison of simple potential functions for simulating liquid water, J. Chem. Phys. 79 (1983) 926–935.
[56] H.J.C. Berendsen, J.P.M. van Postma, W.F. Van Gunsteren, A. DiNola, J.R. Haak, Molecular dynamics with coupling to an external bath, J. Chem. Phys. 81 (1984) 3684–3690.
[57] J. Wang, R.M. Wolf, J.W. Caldwell, P.A. Kollman, D.A. Case, Development and testing of a general amber force field, J. Comput. Chem. 25 (2004) 1157–1174.
[58] T. Darden, D. York, L. Pedersen, Particle mesh Ewald: An N log (N) method for Ewald sums in large systems, J. Chem. Phys. 98 (1993) 10089.
[59] B. Hess, H. Bekker, H.J.C. Berendsen, J.G.E.M. Fraaije, LINCS: A linear constraint solver for molecular simulations, J. Comput. Chem. 18 (1997) 1463–1472.
[60] M. Parrinello, A. Rahman, Polymorphic transitions in single crystals: A new molecular dynamics method, J. Appl. Phys. 52 (1981) 7182–7190.
[61] K. Lindorff-Larsen, S. Piana, K. Palmo, P. Maragakis, J.L. Klepeis, R.O. Dror, D.E. Shaw, Improved side-chain torsion potentials for the Amber ff99SB protein force field, Proteins Struct. Funct. Bioinforma. 78 (2010) 1950–1958.
[62] J.A. Maier, C. Martinez, K. Kasavajhala, L. Wickstrom, K.E. Hauser, C. Simmerling, ff14SB: improving the accuracy of protein side chain and backbone parameters from ff99SB, J. Chem. Theory Comput. 11 (2015) 3696–3713.
[63] J. Huang, S. Rauscher, G. Nawrocki, T. Ran, M. Feig, B.L. De Groot, H. Grubmüller, A.D. MacKerell Jr, CHARMM36m: an improved force field for folded and intrinsically disordered proteins, Nat. Methods. 14 (2017) 71–73.
[64] S. Pronk, S. Páll, R. Schulz, P. Larsson, P. Bjelkmar, R. Apostolov, M.R. Shirts, J.C. Smith, P.M. Kasson, D. Van Der Spoel, GROMACS 4.5: a high-throughput and highly parallel open source molecular simulation toolkit, Bioinformatics. 29 (2013) 845–854.
[65] B. Hess, C. Kutzner, D. Van Der Spoel, E. Lindahl, GROMACS 4: algorithms for highly efficient, load-balanced, and scalable molecular simulation, J. Chem. Theory Comput. 4 (2008) 435–447.
[66] J. Antony, J. Piquemal, N. Gresh, Complexes of thiomandelate and captopril mercaptocarboxylate inhibitors to metallo-β-lactamase by polarizable molecular mechanics. Validation on model binding sites by quantum chemistry, J. Comput. Chem. 26 (2005) 1131–1147.
[67] E.F. Pettersen, T.D. Goddard, C.C. Huang, G.S. Couch, D.M. Greenblatt, E.C. Meng, T.E. Ferrin, UCSF Chimera—a visualization system for exploratory research and analysis, J. Comput. Chem. 25 (2004) 1605–1612.
[68] Y. Demir, H. Ceylan, C. Türkeş, Ş. Beydemir, Molecular docking and inhibition studies of vulpinic, carnosic and usnic acids on polyol pathway enzymes, J. Biomol. Struct. Dyn. 40 (2022) 12008–12021.
[69] J. Gingras, S. Smith, D.J. Matson, D. Johnson, K. Nye, L. Couture, E. Feric, R. Yin, B.D. Moyer, M.L. Peterson, Global Nav1. 7 knockout mice recapitulate the phenotype of human congenital indifference to pain, PLoS One. 9 (2014) e105895.
[70] Y. Yan, D. Zhang, P. Zhou, B. Li, S.-Y. Huang, HDOCK: a web server for protein–protein and protein–DNA/RNA docking based on a hybrid strategy, Nucleic Acids Res. 45 (2017) W365–W373.
[71] R.T. McGibbon, K.A. Beauchamp, M.P. Harrigan, C. Klein, J.M. Swails, C.X. Hernández, C.R. Schwantes, L.-P. Wang, T.J. Lane, V.S. Pande, MDTraj: a modern open library for the analysis of molecular dynamics trajectories, Biophys. J. 109 (2015) 1528–1532.